CFD-DEM Simulation of Heat Transfer in Spout Fluid Beds

Hamed Hoorijani[1,2], Behrad Esgandari[3], Reza Zarghami[1], Rahmat Sotudeh-Gharebagh[1], Navid Mostoufi*[1]

[1] Multiphase Systems Research Lab, School of Chemical Engineering, College of Engineering, University of Tehran, P.O. Box 11155-4563, Tehran, Iran.

[2] Laboratory for Chemical Technology, Center for Sustainable Chemistry, Ghent University, Technologiepark 125, 9052 Ghent, Belgium

[3] Department of Particulate Flow Modelling, Johannes Kepler University, Altenbergerstr. 69, 4040 Linz, Austria

Abstract

It is necessary to study the flow regimes of spout-fluid beds before considering their application in the industry. A three-dimensional computational fluid dynamic coupled with the discrete element method (CFD-DEM) was employed to study the heat transfer of the jet-in-fluidized bed flow, spouting-with-aeration flow, and intermediate/spout-fluidization flow regimes of the spout-fluid bed. To determine the efficiency of heat transfer in these flow regimes, extensive CFD-DEM simulations were conducted along with a heat transfer model. The heat transfer in these flow regimes was investigated using particle temperature distributions, mean convective heat flux, and average particle temperature. Compared to the other flow regimes, the jet-in-fluidized bed flow regime demonstrated a higher degree of heat transfer due to the presence of bubbles in the annulus. Moreover, it was observed that the spouting-with-aeration flow regime exhibits a better convective heat transfer compared to the intermediate/spout-fluidization. The stable and continuous spout

* Corresponding author: mostoufi@ut.ac.ir

channel of the spouting-with-aeration flow regime helps convective heat transfer more than the interrupting spout channel of the intermediate/spout-fluidization.

Keywords: Flow regime; Temperature distribution; CFD-DEM; Heat transfer; Spout-fluid bed.

1. Introduction

A gas-solid spout-fluid bed combines the advantageous characteristics of both fluidized beds and spouted beds, including high mass and heat transfer rates and efficient interphase contact. Obtaining a thorough understanding of particle behavior, hydrodynamics, and heat and mass transfer mechanisms is essential to the successful operation and scale up of these gas-solid contactors. These complex systems have been studied using a variety of techniques [1-4]. In spite of the extensive information that has been obtained through experimental studies regarding spout-fluid beds, measurements are limited in understanding the details of heat transfer due to the complex interactions between gas, particles, and walls. With increasing the computational power, a wide variety of numerical methods have been developed for investigating the stochastic behavior of multiphase flows. Physical phenomena involved in the process must be properly modeled by these numerical methods. It has been demonstrated that each of these methods can be used to model a specific scale of the process in an effective manner. An Eulerian-Lagrangian approach, computational fluid dynamics coupled with discrete element method (CFD-DEM), has proven to be an effective tool for studying the multiphase flows with complex behaviors [5]. In CFD-DEM, a continuum fixed-grid is used to model the gas phase (Eulerian approach), while discrete element method is used to model the particles (Lagrangian approach). The momentum exchange between phases in a CFD-DEM is accomplished through the application of a drag law [1, 6, 7].

The application of CFD-DEM has been established in studying different process units. This method has been applied to study the conical and prismatic spouted beds. Grohn et al. [8] used CFD-DEM to study the fluidization pattern of cylindrical particles in a spouted bed. They employed different drag models for cylindrical particles and showed that the drag model of Sanjeevi et al. [9] can best fits the movement of these particles. They also simulated a commercial scale fluidized bed rotor granulator and reported higher fluidization intensity for cylindrical particles. In another study, Atxutgi et al. [10] investigated the solid mixing in a conical spouted bed using CFD-DEM. Effect of internal draft tubes with different configurations as well as solid types and flow rates on gas and solid mixing were studied. They showed that incorporating a draft tube decreases the bed voidage due to elevated spout level. Moreover, they showed that Internal devices also affect solid cycle time. In their study, they employed a fountain confiner, to address the gas bypassing issue in the conical spouted bed. They solved the gas bypassing, caused by excess gas flow rates with redirecting the radial flow of air, as it exists the spout.

Numerous studies have examined the characteristics of flow regimes of spout-fluidized beds [2, 11, 12]. The hydrodynamic characteristics of various flow regimes within a spout-fluidized bed were investigated by Link et al. [13] through a combination of experimental and modeling approaches. In this study, the flow regimes were determined through the measurement of pressure fluctuations and the application of empirical models by sharp distinctions among the flow patterns. The results were presented as a regime map for the spout-fluidized bed. In another investigation, an analysis of the hydrodynamic characteristics of various flow regimes, including jet-in-fluidized bed, spouting-with-aeration, and intermediate/spout-fluidization, was carried out by the same researchers [14]. This analysis incorporated positron emission particle tracking (PEPT) and discrete particle modeling to delve into particle velocity distribution, solid volume fraction, and pressure

fluctuations in these diverse flow regimes. This study clearly demonstrated the ability of simulation studies in providing a more profound understanding of such complex systems. Hoorijani et al. [15] investigated the hydrodynamic characteristics of jet-in-fluidized bed, spouting-with-aeration, and intermediate/spout-fluidization flow regimes by employing Computational Fluid Dynamics-Discrete Element Method (CFD-DEM) simulations. This investigation was focused on both axial and lateral mixing in these flow regimes. It was found that jet-in-fluidized beds and spouting-with-aeration flow regimes exhibited superior particle mixing characteristics, with axial mixing prevailing over lateral mixing.

In spite of above mentioned investigations on the hydrodynamics of spout fluidized beds, little is known about the heat transfer in each flow regime and the differences between their heat efficiency. In the past decade, different studies were carried out to shed light on the gap of knowledge about heat transfer in spout-fluid beds [16-22]. Patil et al. [19] compared the results of the CFD-DEM simulation with the experimental data obtained by infrared/particle image velocimetry/digital image analysis (IR/PIV/DIA) technique. They studied the cooling of hot particles in a pseudo-2D fluidized bed by implementing new mechanisms of inter-phase heat transfer into the CFD-DEM modeling. Using the IR/PIV/DIV results, they studied the temperature distribution, particle volume fraction and particle volume fluxes in the fluidized bed [23]. In another study [20], they investigated the particle temperature distribution in a bubbling spout fluidized bed with a hot gas injection by a novel model for fluid-particle heat transfer. Brown and Lattimer [21] studied the heat transfer characteristics of fluidized particles by experimentally measuring emitted infrared radiation. A pseudo 2D spout-fluid bed was studied in different flow configurations corresponding to fluidized, spouted and fixed bed states. The temperature of the inlet gas varied with time for each state of the bed. Their results indicated that the greatest amount of energy is

stored in the particles when they flow downward around the gas channel in the annulus. The annulus and spout channel are integral components of a spout fluidized bed. The annulus is the outer region of the spout fluidized bed, surrounding the central spout. It is an area where an auxiliary fluid flows through a series of holes or channels from the wall. The spout channel is the vertical column in the center of the spout fluidized bed. It is responsible for the primary upward flow of gas and particles. In a well-operating spout fluidized bed, the spout channel should maintain its verticality and symmetry.

Saldarriaga et al. [24] studied the heat transfer in a conical spouted bed by analyzing the effect of operation conditions. In their study, the effect of bed height, inlet gas velocity and composition of the mixture of biomass and sand powder on hydrodynamic and bed-to-surface heat transfer were studied. Their results showed a higher heat transfer coefficient from the wall to the spout. This phenomenon can be attributed to the collision of particles in the fountain with the walls above the bed surface. These particles then slide from the inclined column to the beneath the bed surface.

Lichtenegger et al. [22] used recurrence CFD (rCFD) to study the heat transfer in a fluidized bed. Using this novel approach for simulation of recurrent systems, they obtained the simulation results much faster than in a full-CFD simulation. They conducted CFD-DEM simulations for a lab-scale fluidized bed with approximately 57000 and 95000 hot particles and identified the recurrent state of the fluidization. Zhou et al. [25] studied the effect of particle shape using multi-sphere method on the hydrodynamics and heat transfer of a spouted bed. They showed that the prolate spheroids form the largest bubble at the beginning of the spouting and rise the highest. In their study, it was found that the drag force exerted on the prolate particles has a greater effect on their motion than interlocking the particles and particle-particle frictional forces. Moreover, the ellipsoidal spheroids had a better mobility compared to spherical particles because of their rough

surface and nonuniform torques that cause stronger rotational kinetic energy for these particles. The oblate spheroids showed better heat transfer performance due to their large surface area compared to prolate spheroids. Liu et al. [26] investigated the heat transfer in a gas-fluidized bed near the wall. They adopted two different approaches to resolve the temperature distribution near the wall in the CFD-DEM simulation. In the first approach, they imposed a thermal boundary condition for the gas phase energy equation and in the second approach implemented a particle-wall conduction model (PW) for the particle phase. It was shown that the PW model, due to its robustness and the fact that it is insensitive to the changes of the two model parameters, is a better choice for dense gas-fluidized beds.

The spout-fluid bed reactors play a crucial role in numerous chemical and petrochemical processes, often operating at elevated temperatures to facilitate catalytic reactions. Despite their significance, there is a noticeable lack of literature addressing the heat transfer aspects in these reactors. The limited availability of comprehensive studies on heat transfer within spout-fluidized bed reactors has created a knowledge gap in this vital area. Given their widespread use, a thorough understanding of the heat transfer characteristics in these reactors is essential for optimizing their performance and efficiency. The objective of this work is to study the heat transfer characteristics of different flow regimes (spout-with-aeration, jet-in-fluidized bed and spouting-fluidization) in these systems. The coupled CFD-DEM approach was used to evaluate the heat transfer efficiency in different flow regimes by measuring average particle temperature and convective heat transfer rate. Till now, no prior literature can be found that delves into the study of heat transfer characteristics within flow regimes of spout fluid bed reactors. Studies have, however, been reported the heat transfer in a single flow regime [20-22, 25] or methods to enhance the heat transfer efficiency in a spout fluid bed, where mostly an internal tube has been employed in the bed [27, 28]. An extensive time of CFD-DEM simulations was used to analyze the heat transfer associated with various flow regimes. Gas-solid systems can

be studied in detail through CFD-DEM, which provides a more comprehensive understanding of their characteristics.

2. Model description

2.1. CFD-DEM modeling

Simulations in this study were conducted using the coupled CFD-DEM technique. This model consists of three main sections: CFD, DEM, and their coupling. In the CFD section, the continuity and momentum conservation equations are solved in order to obtain pressure and velocity distribution within the gas phase. Next, the drag force is calculated in the coupling section and employed in the DEM section in order to determine the new position of each particle. Following the calculation of particle position, the porosity profile in the bed is revised and returned to the CFD section for continuing calculations in the next time step. Detailed description of the equations and concepts of these models can be found elsewhere [1, 5]. For brevity, the main equations and general description of each model are presented in this section. CFD and DEM sections were handled using open-source packages OpenFOAM [29] and LIGGGHTS [30], respectively. The coupling section was done using CFDEMcoupling open-source code [31]. Heat transfer models were added to the existing CFDEMcoupling code.

2.2. Heat transfer

Total energy balance for the gas phase, neglecting the work performed by the fluid on the particles due to drag, can be obtained using the following equation.

$$\frac{\partial}{\partial t}\left(\varepsilon\rho_g\left(\epsilon_g + K_g\right)\right) + \nabla.\left(\varepsilon\rho_g\vec{u}\left(\epsilon_g + K_g\right)\right) = -\nabla.\varepsilon p\vec{u} + \dot{Q}_{p-g} + \nabla.\varepsilon k_g^{eff}\nabla T_g \qquad (18)$$

Here, ϵ_g is the internal energy and $K_g=\vec{u}^2/2$ is the kinetic energy of unit mass of the gas. The temperature of the fluid phase can be obtained by solving Eq. (18) and using heat capacity of the fluid ($T_g= \epsilon_g/C_g$). Energy transfers from/to particulate phase through conduction and diffusion. Both effects were considered through the model of Syamlal and Gidaspow [32] for gas phase in terms of effective thermal conductivity.

$$k_g^{eff} = \frac{1-\sqrt{1-\varepsilon}}{\varepsilon} k_g \tag{19}$$

The particle-fluid heat transfer model can be obtained by summing the contributions of all particles using a discrete Dirac delta-function [22, 33]:

$$\dot{Q}_{p-g} = \sum_i \pi k_g d_p Nu_p (T_i - T_g)\delta(r - r_i) \tag{20}$$

where k_g, d_p, T_i, T_g and Nu_p are the thermal conductivity of gas, particle diameter, particle and gas temperature and Nusselt number of particles in the system, respectively. The Nusselt number, Nu_p, was evaluated using the Gunn equation [34]:

$$Nu_p = (7 - 10\varepsilon + 5\varepsilon^2)\left[1 + 0.7Re_p^{0.2}Pr^{0.33}\right] + (1.33 - 2.40\varepsilon + 1.20\varepsilon^2)Re^{0.7}Pr^{0.33} \tag{21}$$

In this equation ε is the porosity, *Re* is the Reynolds number and *Pr* is the Prandtl number.

It was assumed that the convective heat transfer is the primary mechanism for heat transfer within the bed. The general energy balance equation of each particle is presented by:

$$\frac{m_p c_p dT}{dt} = \frac{\rho_p V_p C_p dT_i}{dt} = \sum_{\substack{i=1 \\ i\neq j}} \dot{Q}_{i,j} + \dot{Q}_{p-g} + \dot{Q}_{p-wall} + \dot{Q}_{p,rad} \tag{22}$$

In this equation, m_p, ρ_p, V_p and C_p are the mass, density, volume and thermal capacity of particles, respectively. The terms $\sum_{i=1}^{N} \dot{Q}_{i,j}$, $\dot{Q}_{p-g}$, $\dot{Q}_{p-wall}$ and $\dot{Q}_{p,rad}$ are the energy transfer of particle-particle contact, particle-gas contact, particle-wall contact and radiation from the particles in the system, respectively.

Initially particles are at room temperature, so heat transfer through radiation is negligible. It is reported that the heat exchange resulting from particle-particle and particle-wall interactions for each particle is so small compared to the convective heat transfer that considering them in the thermal equation would not significantly affect the temperature of particle in the bed [17, 23]. Overall, it is well-establishes that considering the heat exchange due to convective heat transfer (gas-solid interface) is the predominant mechanism for heat transfer among particles [22, 35]. Based this assumption, the energy balance equation becomes as follows:

$$\rho_p V_p C_p \frac{dT_i}{dt} = \dot{Q}_{p-g} = -\pi k_g d_p N u_p (T_i - T_g) \quad (22)$$

2.3.Gas-wall heat transfer boundary condition

The heat loss for gas-wall contact was considered in the gas phase thermal energy equation by a boundary condition for thickness of the heat transfer boundary layer. The boundary layer can be justified in terms of the heat transfer resistance inherent in thin films smaller than the particle size. As shown in previous studies, due to vigorous mixing and tortuous motion of gas in fluidized beds, most of the heat transfer resistance and temperature gradient occurs very close to the wall [19]. The grid size should be larger than the thickness of this layer such that the film becomes unresolved and the heat transfer from gas to wall can be modeled using the following heat transfer coefficient:

$$h_w = k_g/\delta_l. \quad (22)$$

Here, δ_l is the thickness of the boundary layer in which most of the resistance to heat transfer is happening. Other resistances to heat transfer in the wall are ignored in this work, due to their minor effect compared to the gas layer. The external temperature, or the temperature of other side of the wall, is assumed to be equal to the temperature of the surrounding (T = 20 ℃). Using the above

mentioned heat transfer coefficient, the boundary condition for gas phase at the walls can be considered as:

$$-k_g^{eff}\frac{dT_g}{dx} = h_w(T_w - T_g) \tag{23}$$

The optimal value for the thickness of the boundary layer is 0.007 mm that results in a heat transfer coefficient equal to 350 W/m^{2}K [19]. This value was used for validation of the heat transfer model.

3. Model

In this work, three flow regimes of the spout fluid beds were studied using the model described earlier. These regimes are jet-in-fluidized bed, spouting-with-aeration and intermediate/spout-fluidization flow regimes, which have reported to have more application in industrial applications [36]. Detailed study on the flow regimes using experimental techniques and the flow regime map have been reported in literature [13, 14]. The hydrodynamic validation and full description of the computational fluid dynamics simulations and discrete element method were presented in our previous study in which the hydrodynamic characteristics of these three flow regimes of the 3D spout-fluid bed were investigated [15]. In Table 1, the physical properties of particles and gas are presented along with the numerical parameters used in validation cases and the simulations. In this work, OpenFOAM [29], LIGGGHTS [30] and CFDEMCoupling [31], were used for CFD, DEM and coupling for simulations. These open-source software has demonstrated excellent capabilities for modeling gas-solid systems [2, 22, 37-39]. Each second of CFD-DEM simulation took about 2.3 hours on 8 CPU cores of 2.1 GHz of university cluster (Intel Xeon E5-2620). Figure 1 shows the general algorithm of the heat transfer model used in the simulations. As can be seen in this figure, energy coupling is performed between phases by calculation of $\dot{Q}_{p-f}$ (Eq. 20) after momentum coupling. It is then possible to obtain the particle temperature by solving the

energy conservation equation for each particle in the DEM section, while considering assumptions incorporated into the heat transfer model. The temperature of the fluid is also determined by solving the total energy balance of the fluid at each time step (Eq. 18).

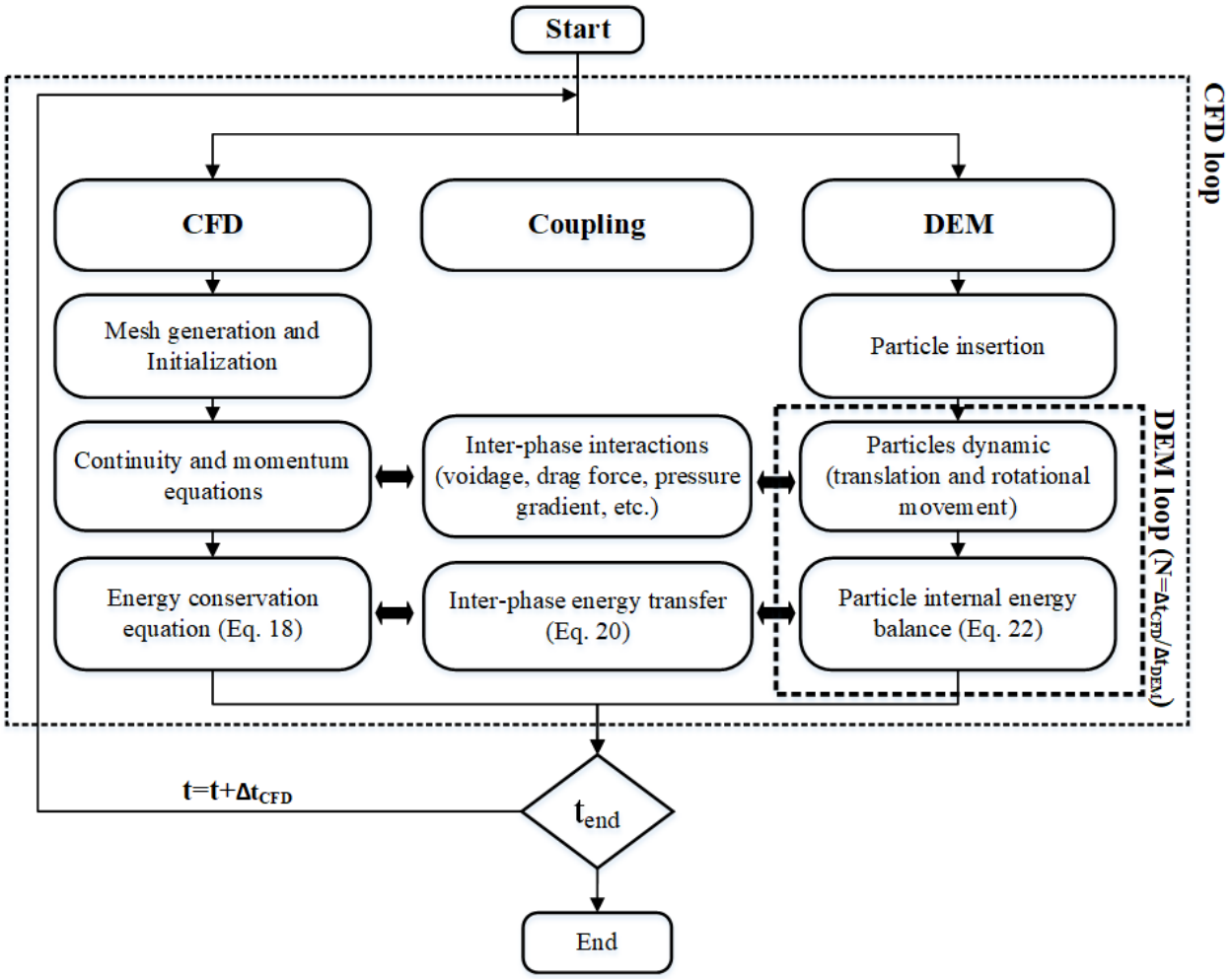

Figure 1. Algorithm of the heat transfer model

The heat transfer model was validated using the experimental data of Patil et al. [19]. Figure 2 shows the schematic of the spout bed considered in the present study. The glass bead particles with diameter of 1 mm and density of 2500 kg/m^3 (Geldart D) at three different inlet gas velocities were considered for this purpose. Initial hot particles at 90 °C were first packed in the bed and

nitrogen gas at 20 ℃ was used as the inlet gas stream to cool down the particles. For heat transfer validation cases, the gas flow rate was considered to be the background gas velocity with no inlet gas from the spout, so that the bed was fluidized using 75 g of the particles (57,324 number of particles). More information about the simulation cases for validation of the heat transfer model are listed in Table 1. In each simulation, uniform hexahedral meshes were used. Based on previous studies [19, 40], the ideal grid size was determined. Simulated and experimental nozzle surfaces were the same for all cases.

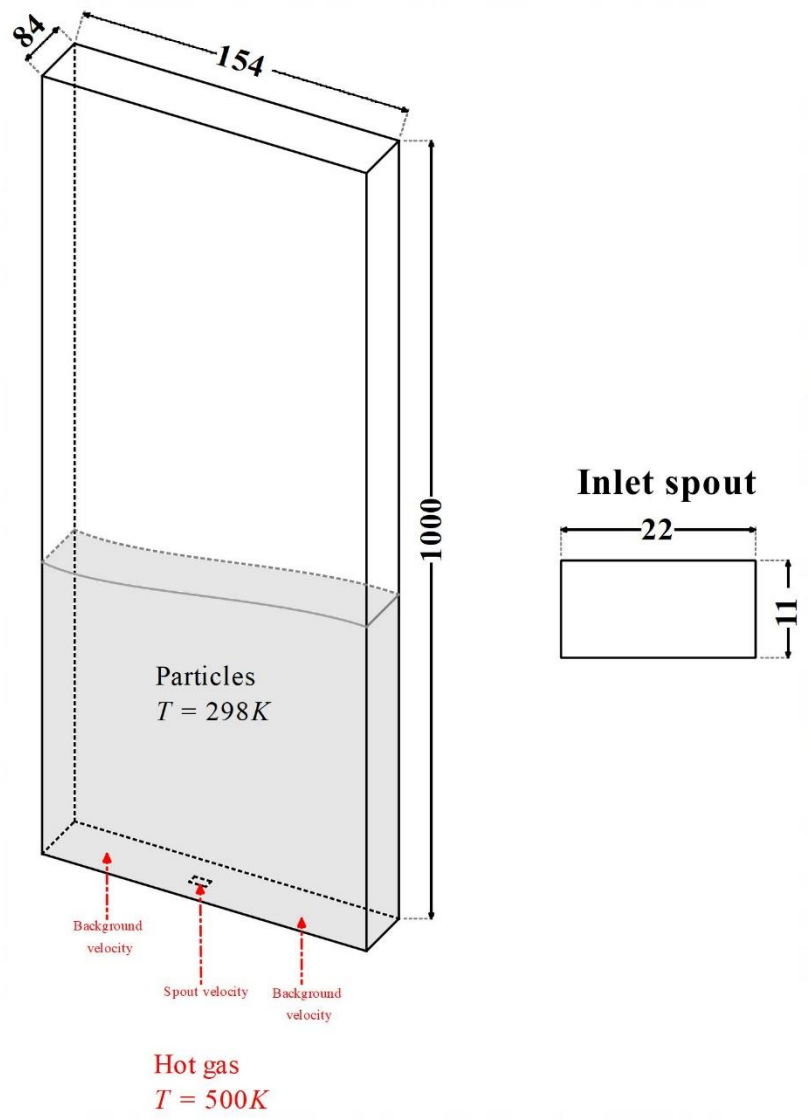

Figure 2. Schematic of the heat transfer simulation. The dimensions are in mm.

Table 1. CFD-DEM simulation parameters

Property	Heat transfer validation case	Simulation cases
Reference	Patil et al. [19]	Link et al. [14]
Particle diameter (mm)	1	4.04
Particle density (kg/m^3)	2500	2526
Gas viscosity (Pa.s)	2×10^{-5}	2.672×10^{-5}
Gas density (kg/m^3)	1.225	0.705

Thermal conductivity of particles (W/m.K)	1.4		1.4	
Specific heat capacity of particles (J/kg.K)	840		840	
Specific heat capacity of gas (J/kg.K)	1010		1031	
Weight of the bed (g)	75		-	
Number of particles	57324		44800	
Young modulus (Pa)	1×10^{7}		1×10^{7}	
Normal restitution coefficient	0.97		0.97	
Passion ratio	0.45		0.45	
Drag model	Tenneti et al. [41]		Tenneti et al. [41]	
Initial particle temperature (K)	363		298	
Coefficient of friction	p-p	0.1	p-p	0.1
	p-w	0.3	p-w	0.3
Coefficient of rolling friction	0.125		-	
Time step (s)	CFD	1×10^{-4}	CFD	8×10^{-5}
	DEM	4×10^{-6}	DEM	4×10^{-6}
Coupling interval	25		20	
Inlet gas temperature (K)	298		500	
Inlet gas velocity (m/s)	U_{bg}	1.2, 1.54, 1.71	U_{bg}	2, 2.5, 3.5
	U_{sp}	0	U_{sp}	90, 60, 65
Minimum fluidization velocity (m/s)	0.58		1.77	
Geometry (mm)	80×15×250		154×84×1000	
Number of cells (x×y×z)	40 × 6 × 100		21 × 14 × 100	

4. Results and discussion

4.1.Validation

As mentioned in previous sections, the validation of the heat transfer model of this study was done by the experimental data of the Patil et al. [19] on cooling of hot particles in a fluidized bed. Figure 3 illustrates the average temperature of particles at three different inlet gas velocities, for

both model and experimental. Details of the particle properties and operating conditions of simulation cases can be found in Table 1. As can be seen in this figure, the average temperature of the particles in the bed decreases with time due to convective heat transfer between the particles and the cold inlet gas. It is also shown in this figure that the model can predict the average temperature of particles at different gas velocities with good agreement with respect to the experimental data with a correlation coefficient (R^2) of 0.998. A slight difference between the experimental results of average particle temperature with computed results can be seen in this figure for each inlet velocity. The difference between the values can be related to the assumption made in this work, for considering the convection as the only mechanism of heat transfer.

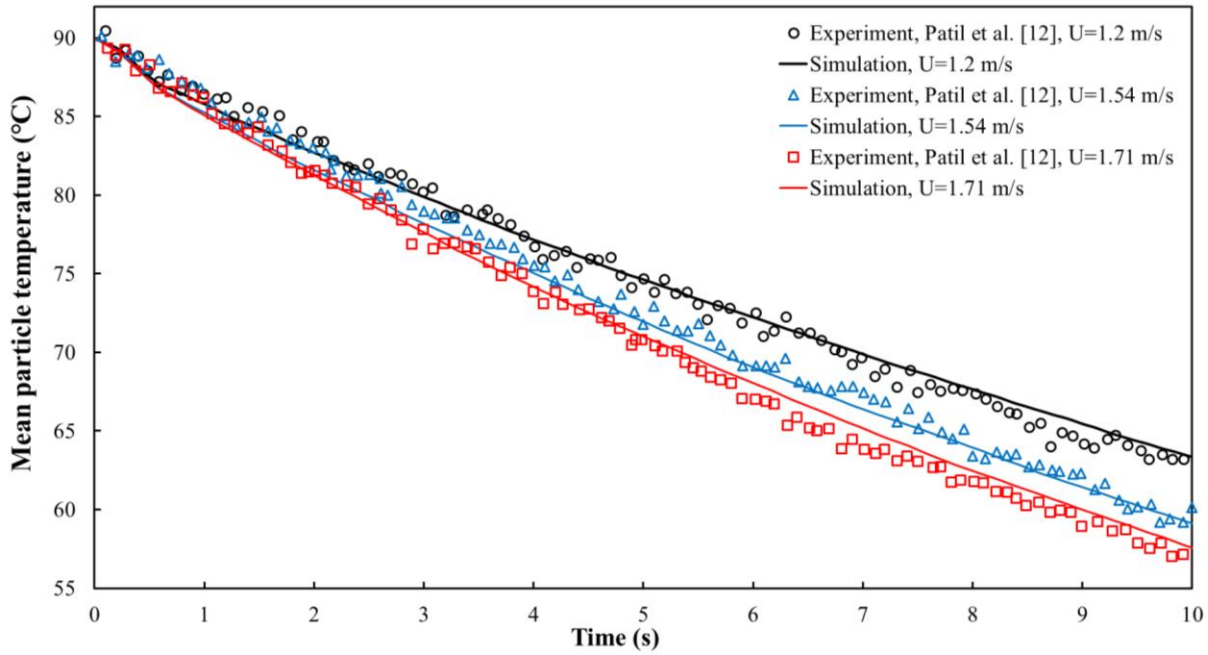

Figure 3. Validation of the heat transfer model with experiment data of Patil et al. [19] for the glass bead particles of 1 mm diameter and density of 2500 kg/m^3

Figure 4 shows the snapshot of the temperature distribution for 1 mm particles at inlet gas velocity of 1.2 m/s. As can be seen in this figure, the model can properly predict the experimental

temperature distribution reported by Patil et al. [19]. It can be seen in Figure 4 that there is a lower temperature at the center of the inlet plate as a result of the colder inlet gas used on the rest of the inlet plate. At the location of spout, no inlet gas was considered, as in the experiments conducted by Patil et al. [19]. As the inlet gas converges over the spout section of the bed, the center of the inlet plate becomes colder. As can be seen in this figure, although the pattern of simulated temperature distribution is similar to the measured profile, values of experimental temperature are lower than in the simulation. Patil et al. [19] measured the temperature by an infrared camera in front and from the surface of the bed. Therefore, this difference can be attributed to the fact that the model shows the local temperature (inside the bed) and not on the surface. The temperature derivations within the bed also can be attributed to the errors of the measurement equipment, analysis and numerical technique and the models employed.

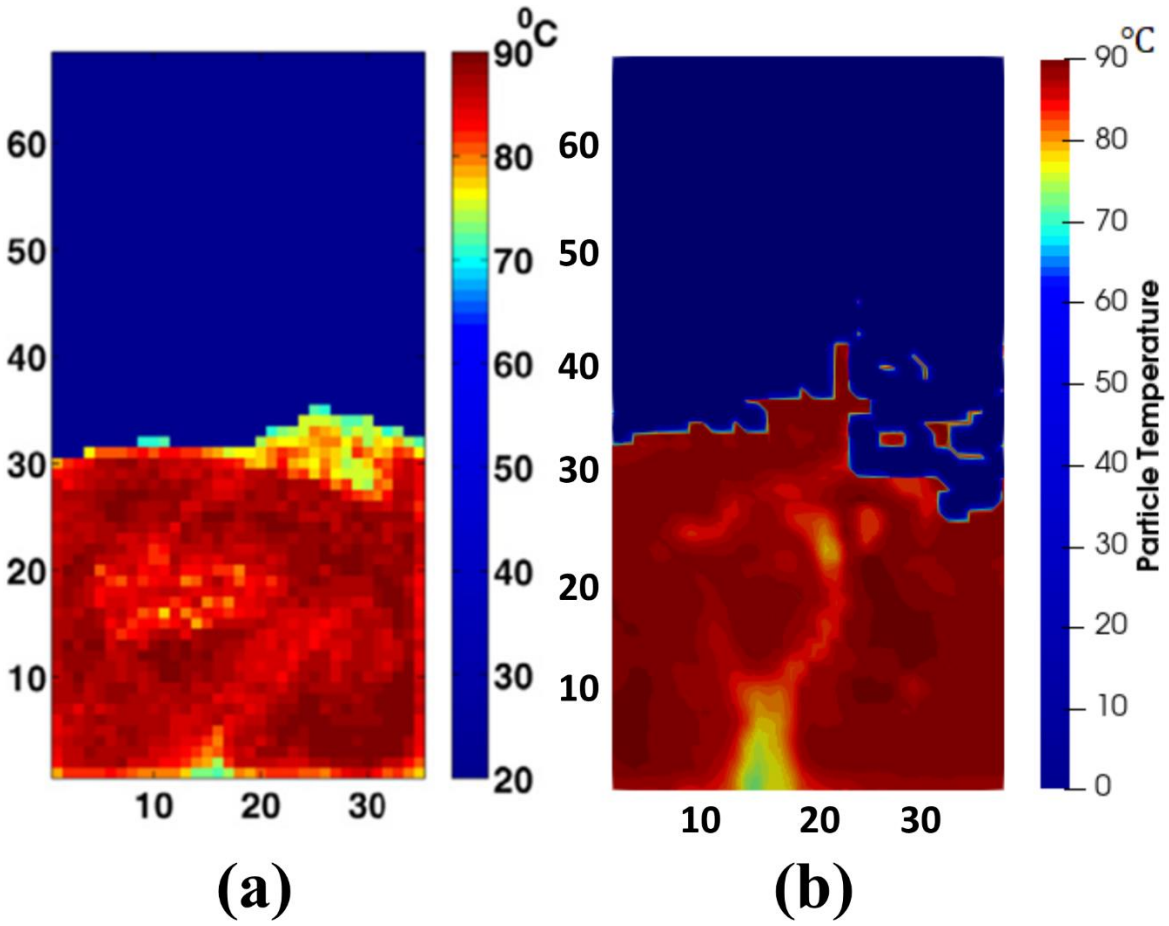

Figure 4. Temperature distribution of particles at inlet gas velocity of 1.2 m/s (a) Patil et al. [19] (b) This study

Solid volume fraction of particles for the experiments and simulations are shown in Figure 5. As can be seen in this figure, there is a good agreement between the experimental results reported by Patil et al. [19] and the simulation of this work. The slight difference between the results can be attributed to the errors of the measurement system as well as the numerical methods employed in the simulations.

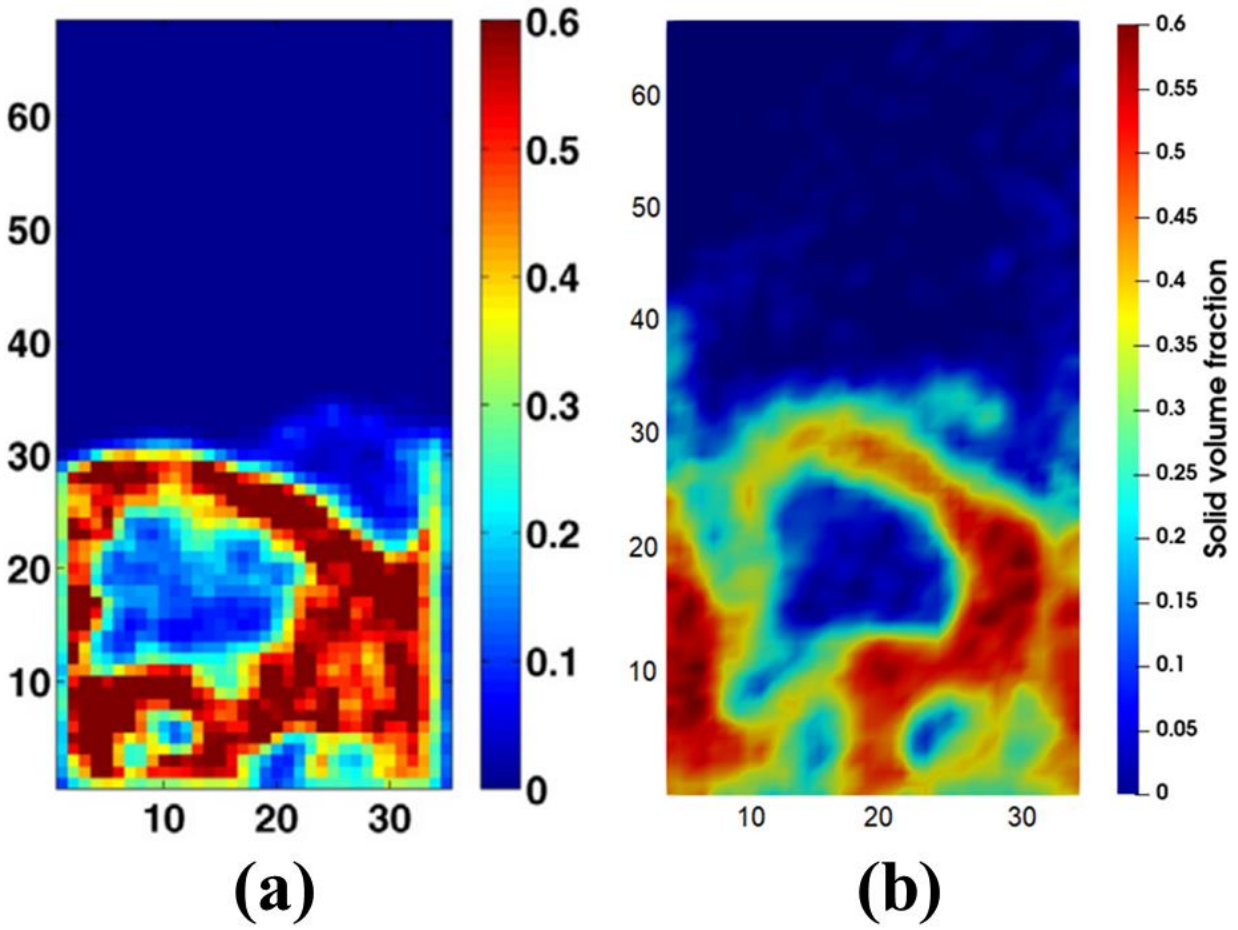

Figure 5. Solid volume fraction distribution of particles at inlet gas velocity of 1.2 m/s (a) Patil et al. [19] (b) This study

Detailed hydrodynamic study and validation of the model have been carried out in a previous work [15]. Figure 6 shows the time-average vertical velocity of flow regimes studied in this work with experimental results reported in Link et al. [14]. As can be seen in this figure, the model can predict the vertical velocity of particle accurately compared to the experimental data. The results indicate that at the center of the bed, the time averaged vertical velocity is higher for the spouting-with-aeration, jet-in-fluidized bed and intermediate/spout-fluidization flow regimes, respectively. This trend can be related to the steady spout channel of the spouting-with-aeration and

the small bubbles in the annulus of the jet-in-fluidized-bed flow regimes, respectively. As can be seen in Figure 6, the above mentioned flow regimes have higher time-averaged vertical velocity compared to the interrupted spout channel of the intermediate/spout-fluidization flow regime. Therefore, this figure demonstrates the ability of the model to predict the hydrodynamic characteristics of these gas-solid systems.

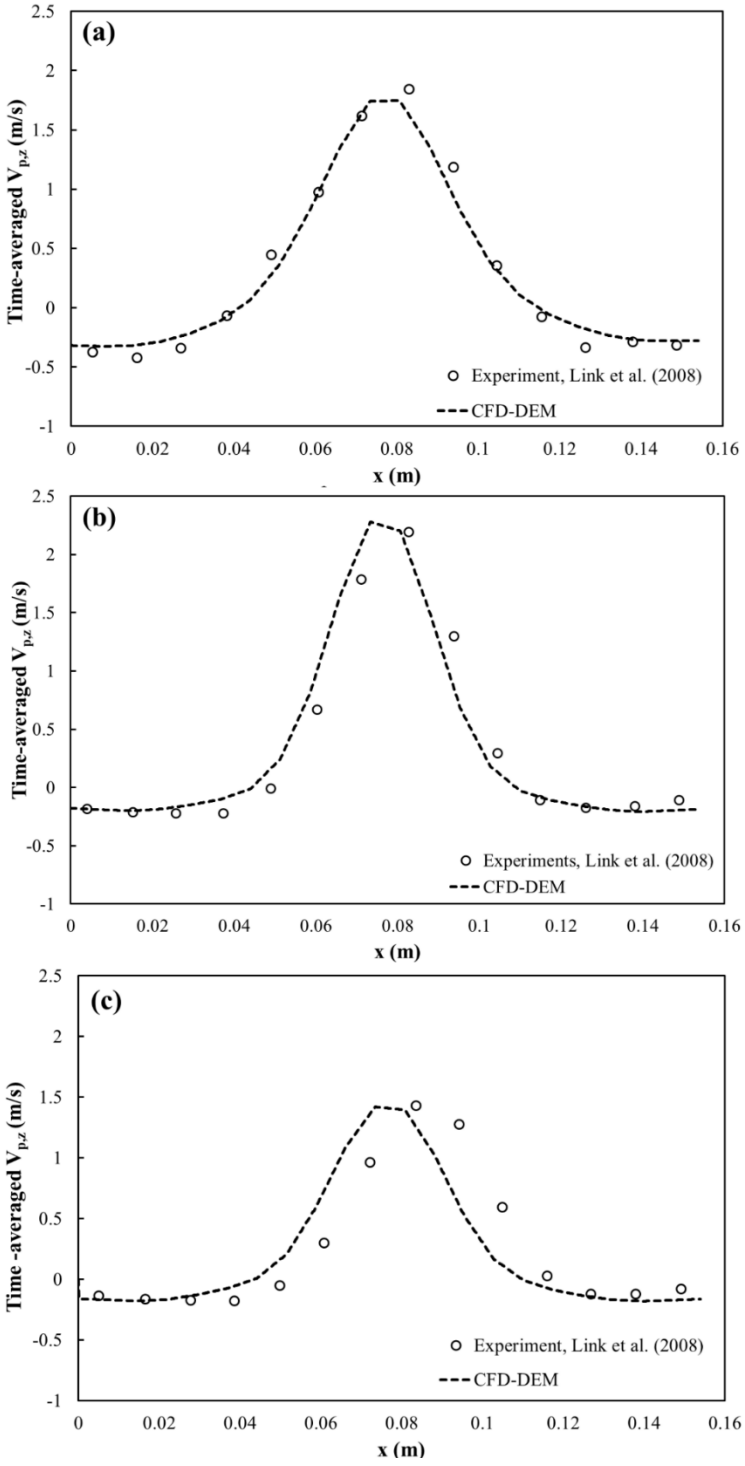

Figure 6. Time-averaged vertical velocity of particles at the height of 15 cm of the bed for (a) jet-in-fluidized bed (b) spouting-with-aeration (c) intermediate/spout-fluidization

Figure 7 shows the time-averaged solids volume fraction in various flow regimes at two different heights of the spout-fluid bed. As can be seen in this figure, the solids fraction at the center is lower in the jet-in-fluidized bed and spouting-with-aeration flow regimes, which indicates the existence of a stable spout channel in these flow regimes compared to the intermediate/spout-fluidization flow regime, as also mentioned by other researchers [14, 15]. Also, in the annulus region close to the walls, the solids fraction is lower in the jet-in-fluidized bed flow regime compared to the other flow regimes. This can be attributed to the existence of small bubbles in the annulus region in the jet-in-fluidized bed flow regime, resulting in enhanced particle circulation and more uniform heat transfer in the annulus region.

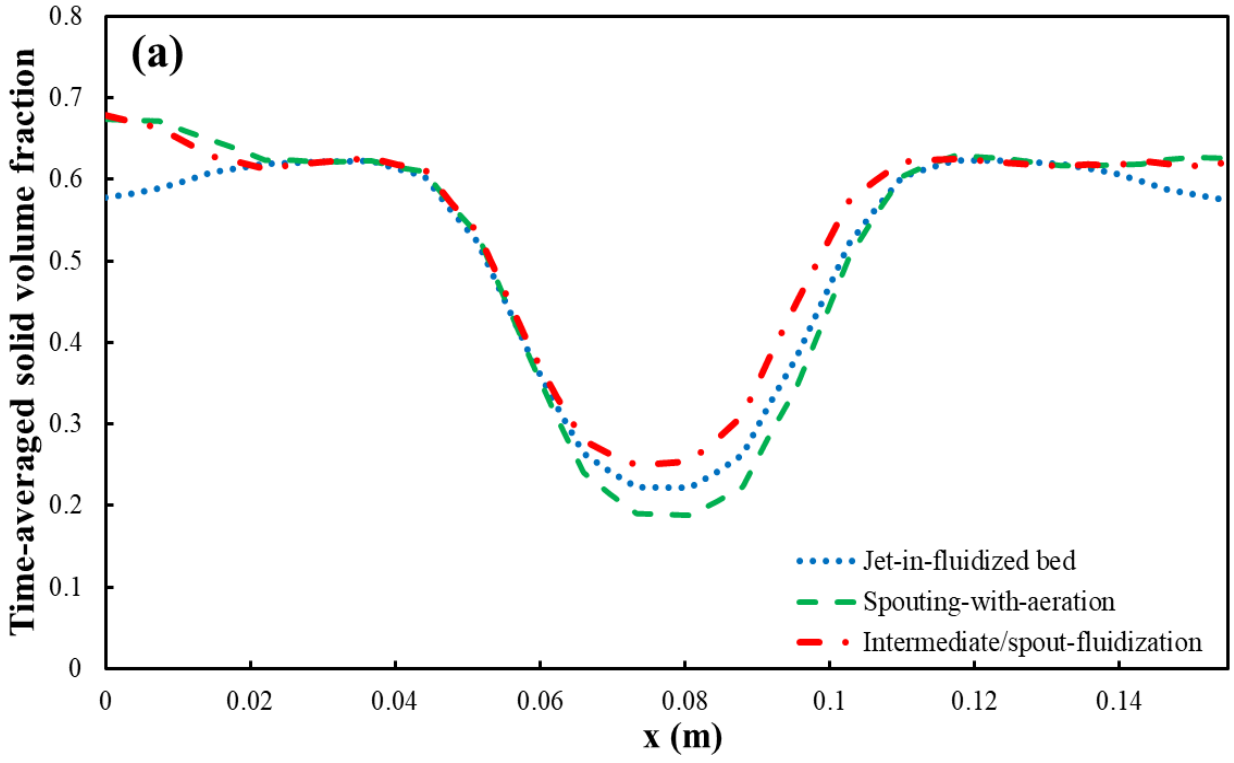

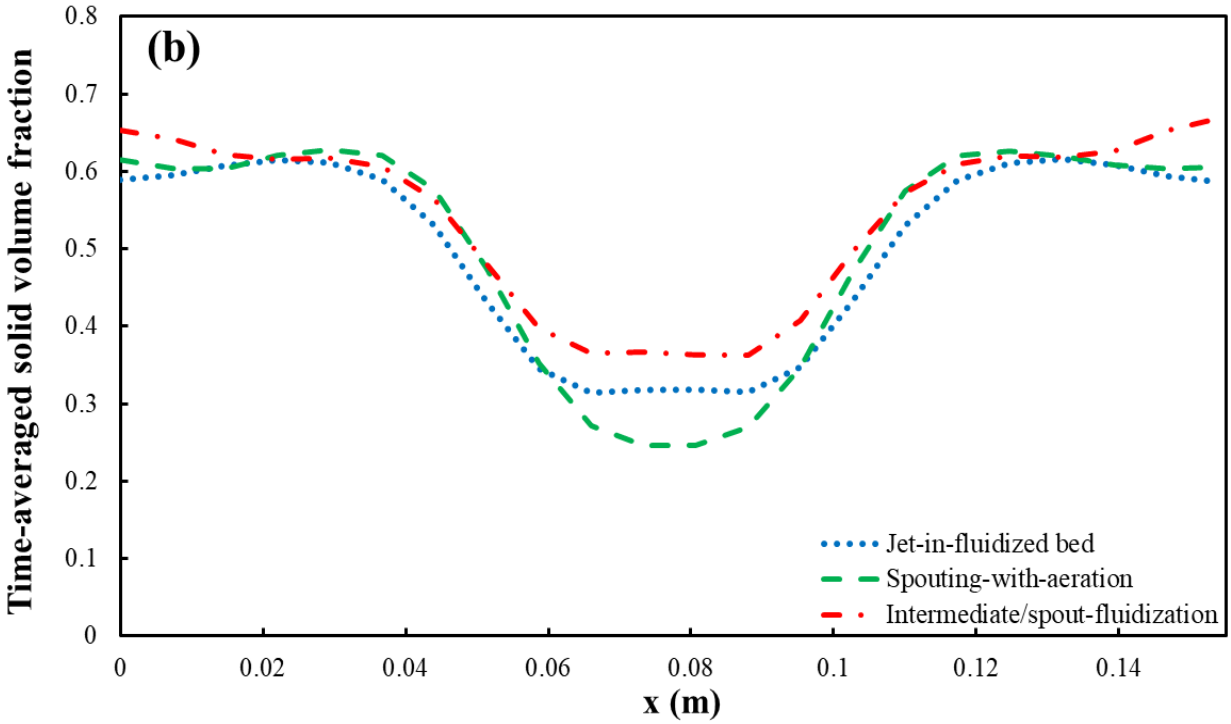

Figure 7. Time-averaged solids volume fraction in different flow regimes at heights of (a) 0.075 m (b) 0.15 m above the inlet spout

4.2. Heat transfer rate

Figure 8 shows the average convective heat flux for three flow regimes with hot gas with the temperature of 223 ℃ (500 K) as inlet and particles initially at room temperature 25 ℃ (298 K). At the beginning of the process, there is a high temperature difference between the hot gas and cold particles that causes a high driving force for the interphase heat transfer. As the process continues, the system moves toward thermal equilibrium and the rate of convective heat flux decreases in all flow regimes. The jet-in-fluidized bed regime benefits from both a spout channel and bubbles in the annulus [14]. The existence of bubbles in the annulus region leads to a higher level of interaction between the cold particles and the hot gas in this regime, resulting in a higher convective heat flux. The spouting-with-aeration regime has a continuous and stable spout channel that penetrates the entire bed [14]. The continuous spout ensures the slow and continuous

movement of particles through the annulus towards the spout channel, preserving the particle configuration in the bed. This difference occurs due to the fact that the convective heat flux is higher than in the intermediate/spout-fluidization regime. In the intermediate/spout-fluidization, particles from the annulus periodically block the intermittent spout channel [14]. When the spout channel is closed halfway, the bubbles will form in the bottom half to help opening the blocked channel. Thus, the convective heat flux for this regime decreases due to this cycle, which increases the time required for thermal equilibrium to be reached.

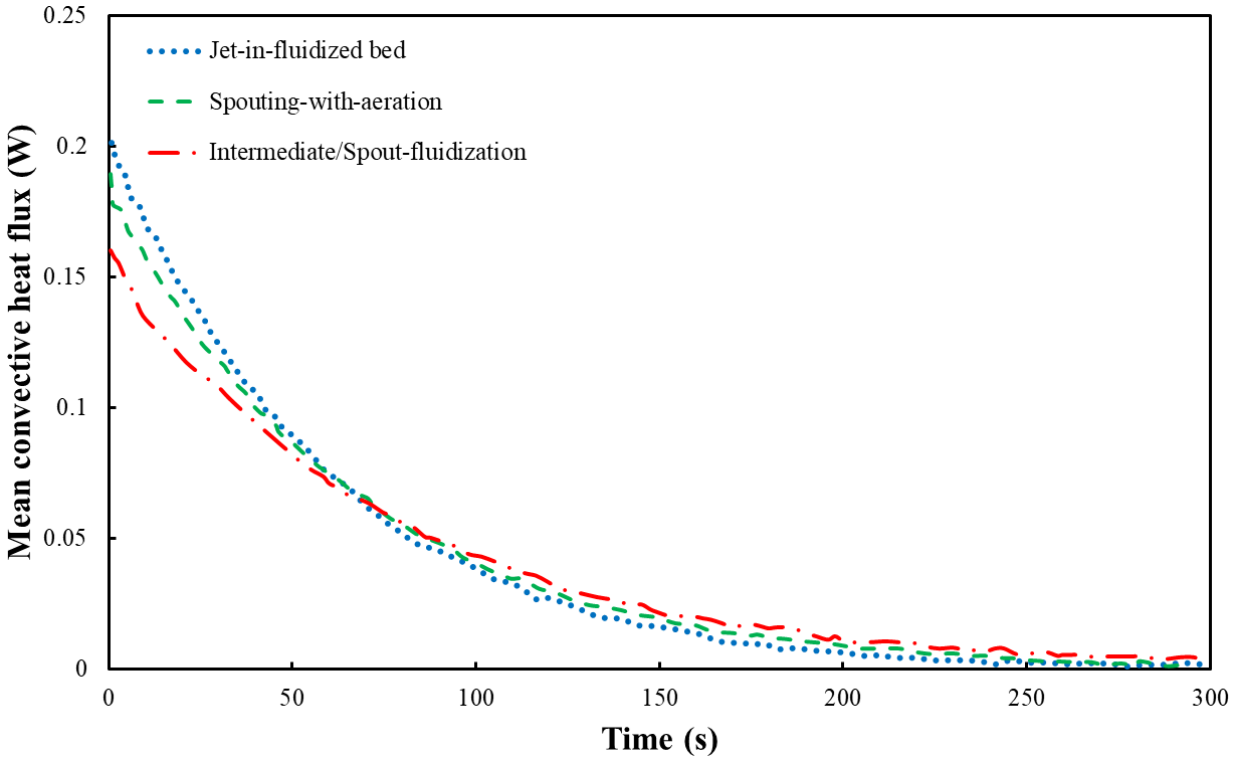

Figure 8. Average convective heat flux in various flow regimes

4.3. Temperature distribution

Figure 9 shows the snapshots of particle temperature distribution of each flow regime at different simulation times. As can be seen in this figure, the temperature in the particulate phase increases with time. At each time step, the particle phase in the spout exhibits a higher temperature

in all regimes due to the exposure to the hot inlet gas. As it can be seen, the convection is the main mechanism of heat transfer between the phases in the bed. The jet-in-fluidized bed and spouting-with-aeration flow regimes exhibit a higher rate for temperature change over time. Formation and eruption of bubbles in the jet-in-fluidized bed regime and the continuous spout channel through the entire bed in the spouting-with-aeration enhances the convective heat transfer rate. Moreover, as a result of higher convection, the particle phase temperature in the spout channel for the jet-in-fluidized bed and spouting-with-aeration is higher. Additionally, the dead zones of the spout-fluidized bed show higher temperatures during the process. In these regions, the particles are stagnant and constantly undergo heat exchange with the gas.

Time	Jet-in-fluidized bed	Spouting-with-aeration	Intermediate/Spout-fluidization
1 s	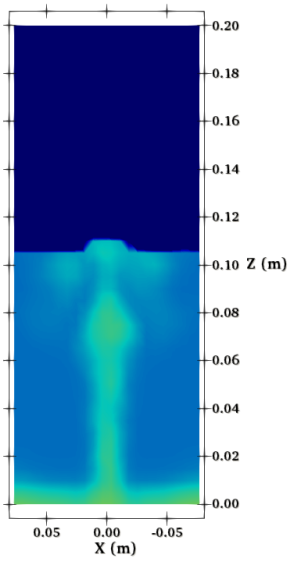	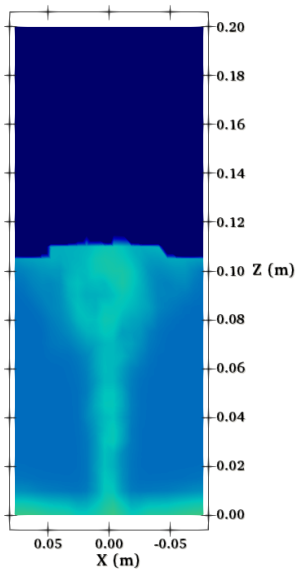	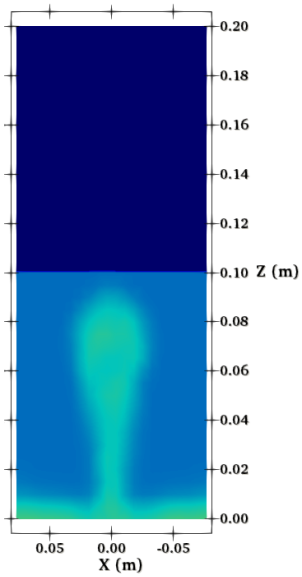

5 s

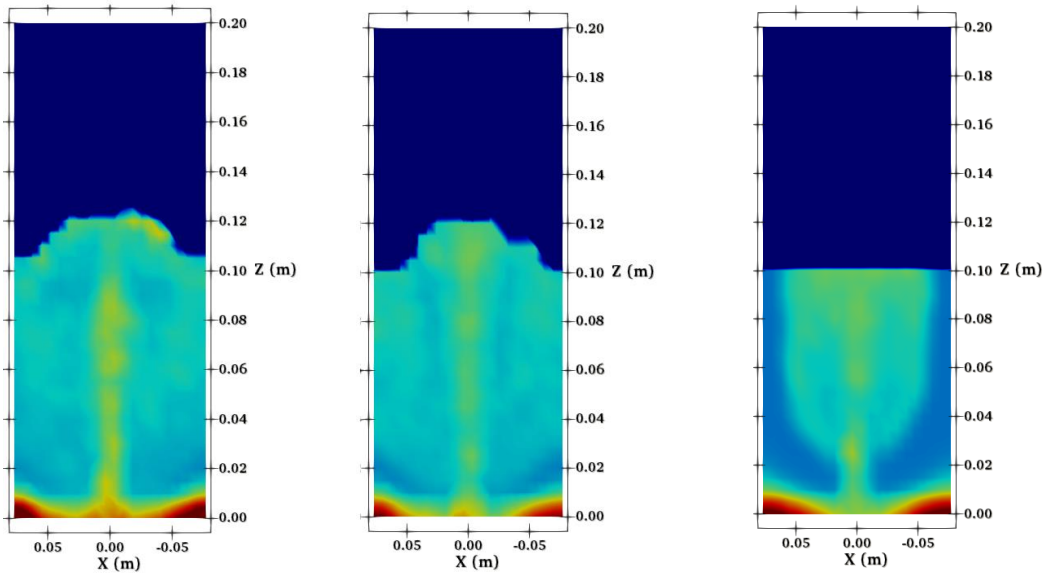
0.20
0.18
0.16
0.14
0.12
0.10 Z (m)
0.08
0.06
0.04
0.02
0.00
0.05 0.00 -0.05
X (m)

10 s

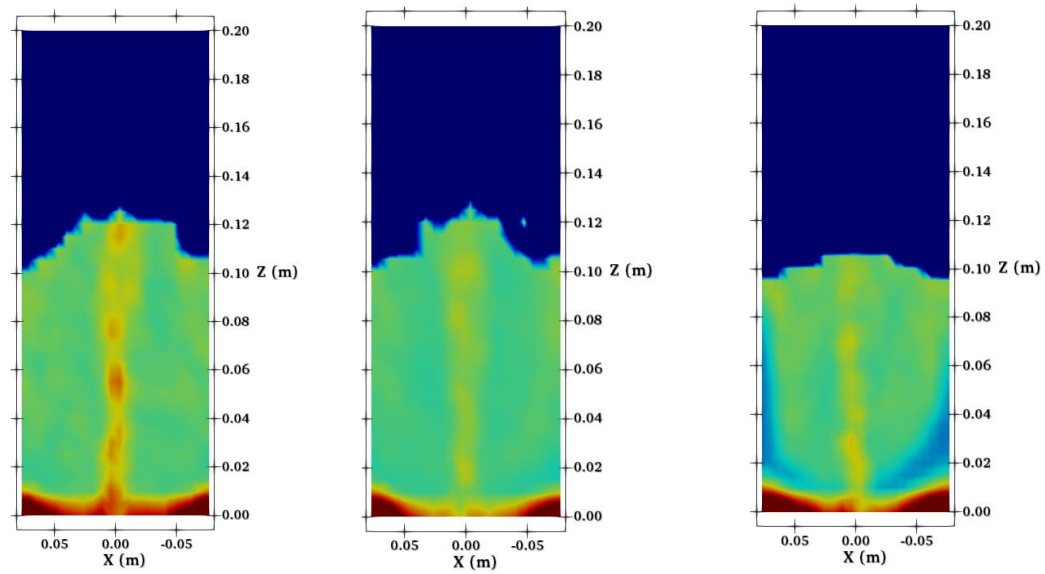
0.20
0.18
0.16
0.14
0.12
0.10 Z (m)
0.08
0.06
0.04
0.02
0.00
0.05 0.00 -0.05
X (m)

15 s

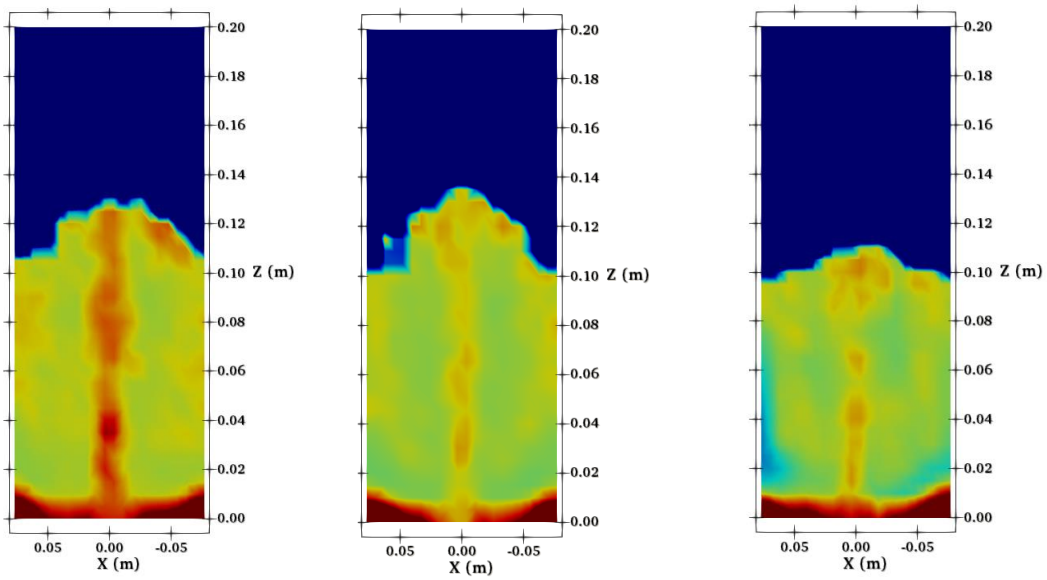
0.20
0.18
0.16
0.14
0.12
0.10 Z (m)
0.08
0.06
0.04
0.02
0.00
0.05 0.00 -0.05
X (m)

20 s

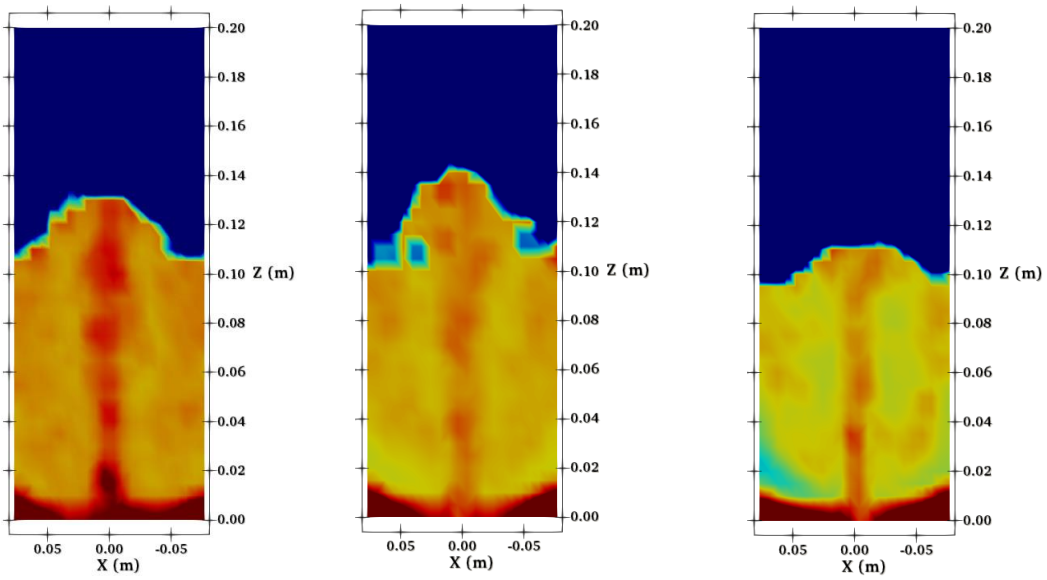
0.20
0.18
0.16
0.14
0.12
0.10 Z (m)
0.08
0.06
0.04
0.02
0.00
0.05 0.00 -0.05
X (m)

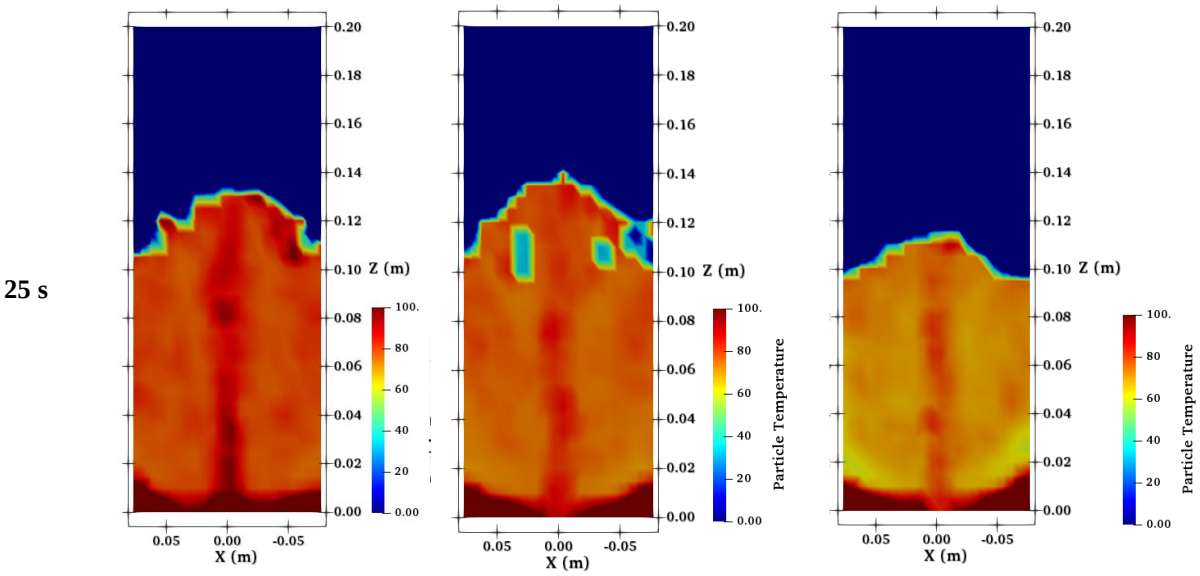

Figure 9. Temperature distribution of the particle phase at different time steps for various flow regimes

4.4. Temperature profile

Figure 10 shows the mean particle temperature for each flow regimes with 4.04 mm glass bead particles at initial temperature of 25 ℃ (298 K) and hot inlet gas of 223 ℃ (500 K). This figure illustrates that the mean particle temperature increases with time in all flow regimes. As mentioned in the previous section, the jet-in-fluidized bed, the spouting with aeration, and the intermediate/spout-fluidization flow regimes have greater heat transfer rates, respectively. As illustrated in Figure 10, the jet-in-fluidized bed reaches equilibrium temperature (temperature of 187 ℃) more quickly. As explained in previous sections, the jet-in-fluidized bed regime has a higher gas-solid interaction due to the existence of bubbles and spout channel at the same time in the bed. This causes a higher heat transfer rate between the two phases and the bed reaches the final temperature (thermal equilibrium state) faster than in other regimes. As shown in Figure 8, the spouting-with-aeration regime results in a faster rise of mean particle temperature in the steady

spout channel in comparison with the intermediate/spout-fluidization regime, which in turn results in a higher convective heat transfer rate. Consequently, achieving the thermal equilibrium state is quicker in spouting-with-aeration regime than in the intermediate/spout-fluidization regime.

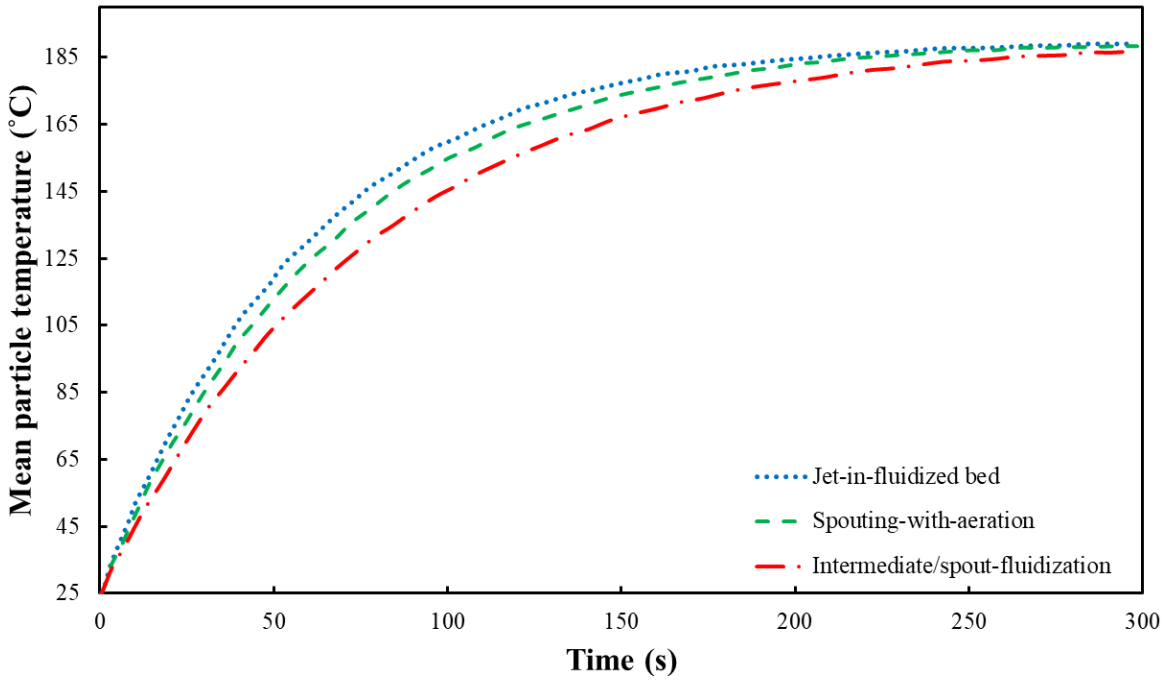

Figure 10. Mean particle temperature for three flow regimes

Conclusions

Heat transfer characteristics of the jet-in-fluidized bed, the spouting-with-aeration and the intermediate/spout-fluidization flow regimes of a spout-fluid bed were studied. The heat transfer model was validated using existing experimental results. It was assumed that the convection is the main source of energy transfer between phases and the diffusive heat transfer can be neglected. The study of average heat transfer rate and particle temperature in the regimes, suggested that the jet-in-fluidized bed has a higher heat transfer rate in comparison with the other flow regimes. The formation and movement of bubbles in the annulus helps the energy transfer by convection which was considered as the main mechanism of heat transfer. Moreover, the spouting-with-aeration

regime showed a better heat transfer rate due to its continuous and stable spout channel than the intermediate/spout-fluidization regime. The particle temperature showed that due to the convective heat transfer mechanism, the particles in the spout channel have the highest temperature during the process. Also, dead zones in the spout-bed have higher temperatures in the process since they are constantly exposed to convective heat transfer with the gas.

Nomenclature

e	Coefficient of restitution of particle i
C_g	Gas heat capacity ($m^2 \cdot s^{-2} \cdot K^{-1}$)
d_p	Particle diameter (m)
g	Gravity ($m \cdot s^{-2}$)
h_w	Convective heat transfer coefficient ($kg \cdot s^{-3} \cdot K^{-1}$)
K_g	Kinetic energy ($kg \cdot m^2 \cdot s^{-2}$)
k_g	Gas thermal conductivity ($kg \cdot m \cdot s^{-3} \cdot K^{-1}$)
k_g^{eff}	Effective thermal conductivity ($kg \cdot m \cdot s^{-3} \cdot K^{-1}$)
m_i	Mass of the particle i^{th} (kg)
Nu_p	Nusselt number
$\dot{Q}_{p-f}$	Particle – fluid heat transfer ($kg \cdot m^2 \cdot s^{-3}$)
T_g	Gas temperature (K)
Re_p	Reynolds number ($d_p \varepsilon \rho_g \lvert u_g - u_p \rvert / \mu$)
T_i	Particle temperature (K)
u_p	Particle velocity ($m \cdot s^{-1}$)
$\vec{u}$	Gas velocity vector ($m \cdot s^{-1}$)
Y_i	Young's modulus (Pa)

Greek letters

δ_l	Thickness of the heat transfer boundary layer (m)
ε	Porosity
ϵ_g	Internal energy ($kg \cdot m^2 \cdot s^{-2}$)
μ	Gas dynamic viscosity ($kg \cdot m^{-1} \cdot s^{-1}$)
ρ_g	Density of gas ($kg \cdot m^{-3}$)
∇p	Pressure gradient ($Pa \cdot m^{-1}$)

Reference

[1] S. Golshan, R. Sotudeh-Gharebagh, R. Zarghami, N. Mostoufi, B. Blais, J.A.M. Kuipers, Review and implementation of CFD-DEM applied to chemical process systems, Chemical Engineering Science, 221 (2020) 115646.

[2] B. Esgandari, S. Golshan, R. Zarghami, R. Sotudeh-Gharebagh, J. Chaouki, CFD-DEM analysis of the spouted fluidized bed with non-spherical particles, The Canadian Journal of Chemical Engineering, 99 (2021) 2303-2319.

[3] S.A. Solovev, O.V. Soloveva, D.L. Paluku, A.A. Lamberov, CFD simulation of the ethylbenzene dehydrogenation reaction in the fixed bed reactor with a cylindrical catalyst of various sizes, Chemical Product and Process Modeling, 17 (2022) 583-602.

[4] B. Patro, K.K. Kumar, D.J. Krishna, Computational fluid dynamics studies of gas-solid flows in a horizontal pipe, subjected to an adiabatic wall, using a variable gas properties Eulerian model, Chemical Product and Process Modeling, 14 (2019).

[5] H.R. Norouzi, R. Zarghami, R. Sotudeh-Gharebagh, N. Mostoufi, Coupled CFD-DEM modeling: formulation, implementation and application to multiphase flows, John Wiley & Sons, 2016.

[6] N.G. Deen, M. Van Sint Annaland, M.A. Van der Hoef, J.A.M. Kuipers, Review of discrete particle modeling of fluidized beds, Chemical Engineering Science, 62 (2007) 28-44.

[7] H.R. Norouzi, S. Golshan, R. Zarghami, On the drag force closures for multiphase flow modeling, Chemical product and process modeling, 17 (2022) 531-582.

[8] M. Tellabide, I. Estiati, A. Atxutegi, H. Altzibar, R. Aguado, M. Olazar, Fine particle flow pattern and region delimitation in fountain confined conical spouted beds, Journal of Industrial and Engineering Chemistry, 95 (2021) 312-324.

[9] S.K.P. Sanjeevi, J.A.M. Kuipers, J.T. Padding, Drag, lift and torque correlations for non-spherical particles from Stokes limit to high Reynolds numbers, International Journal of Multiphase Flow, 106 (2018) 325-337.

[10] A. Atxutegi, P. Kieckhefen, S. Pietsch-Braune, R. Aguado, J. Bilbao, S. Heinrich, M. Olazar, Solid-fluid mixing behavior of conical spouted beds with internal devices, Advanced Powder Technology, 34 (2023) 104136.

[11] S. Golshan, B. Esgandari, R. Zarghami, CFD-DEM and TFM Simulations of a Spouted Bed, Chemical Engineering Transactions, 57 (2017) 1249-1254.

[12] B. Esgandari, S. Rauchenzauner, C. Goniva, P. Kieckhefen, S. Schneiderbauer, A comprehensive comparison of Two-Fluid Model, Discrete Element Method and experiments for the simulation of single- and multiple-spout fluidized beds, Chemical Engineering Science, 267 (2023) 118357.

[13] J.M. Link, L.A. Cuypers, N.G. Deen, J.A.M. Kuipers, Flow regimes in a spout–fluid bed: A combined experimental and simulation study, Chemical Engineering Science, 60 (2005) 3425-3442.

[14] J. Link, N. Deen, H. Kuipers, X. Fan, A. Ingram, D. Parker, J. Wood, J.P.K. Seville, PEPT and discrete particle simulation study of spout-fluid bed regimes, AIChE Journal, 54 (2008) 1189-1202.

[15] H. Hoorijani, B. Esgandari, R. Zarghami, R. Sotudeh-Gharebagh, N. Mostoufi, Comparative CFD-DEM study of flow regimes in spout-fluid beds, Particuology, 85 (2024) 323-334.

[16] H. Wu, N. Gui, X. Yang, J. Tu, S. Jiang, Numerical simulation of heat transfer in packed pebble beds: CFD-DEM coupled with particle thermal radiation, International Journal of Heat and Mass Transfer, 110 (2017) 393-405.

[17] Z.Y. Zhou, A.B. Yu, P. Zulli, A new computational method for studying heat transfer in fluid bed reactors, Powder Technology, 197 (2010) 102-110.

[18] L. Lu, A. Morris, T. Li, S. Benyahia, Extension of a coarse grained particle method to simulate heat transfer in fluidized beds, International Journal of Heat and Mass Transfer, 111 (2017) 723-735.

[19] A. Patil, E.A.J.F. Peters, H. Kuipers, Comparison of CFD-DEM heat transfer simulations with infrared/visual measurements, Chemical Engineering Journal, 277 (2015) 388-401.

[20] A.V. Patil, E.A.J.F. Peters, J.A.M. Kuipers, Computational study of particle temperature in a bubbling spout fluidized bed with hot gas injection, Powder Technology, 284 (2015) 475-485.

[21] S.L. Brown, B.Y. Lattimer, Transient gas-to-particle heat transfer measurements in a spouted bed, Experimental Thermal and Fluid Science, 44 (2013) 883-892.

[22] T. Lichtenegger, E.A.J.F. Peters, J.A.M. Kuipers, S. Pirker, A recurrence CFD study of heat transfer in a fluidized bed, Chemical Engineering Science, 172 (2017) 310-322.

[23] A.V. Patil, E.A.J.F. Peters, V.S. Sutkar, N.G. Deen, J.A.M. Kuipers, A study of heat transfer in fluidized beds using an integrated DIA/PIV/IR technique, Chemical Engineering Journal, 259 (2015) 90-106.

[24] J.F. Saldarriaga, J. Grace, C.J. Lim, Z. Wang, N. Xu, A. Atxutegi, R. Aguado, M. Olazar, Bed-to-surface heat transfer in conical spouted beds of biomass–sand mixtures, Powder Technology, 283 (2015) 447-454.

[25] D. E, P. Zhou, S. Guo, J. Zeng, J. Cui, Y. Jiang, Y. Lu, Z. Jiang, Z. Li, S. Kuang, Particle shape effect on hydrodynamics and heat transfer in spouted bed: A CFD–DEM study, Particuology, 69 (2022) 10-21.

[26] X. Liu, N.G. Deen, Y. Tang, On the treatment of bed-to-wall heat transfer in CFD-DEM simulations of gas-fluidized beds, Chemical Engineering Science, 236 (2021) 116492.

[27] Y. Yue, S. Wang, Y. Shen, Gas-solid mixing and heat transfer performance in alternating spout deflection, Chemical Engineering Science, 234 (2021) 116446.

[28] Y. Yue, T. Wang, M. Sakai, Y. Shen, Particle-scale study of spout deflection in a flat-bottomed spout fluidized bed, Chemical Engineering Science, 205 (2019) 121-133.

[29] H.G. Weller, G. Tabor, H. Jasak, C. Fureby, A tensorial approach to computational continuum mechanics using object-oriented techniques, Computers in physics, 12 (1998) 620-631.

[30] C. Kloss, C. Goniva, LIGGGHTS – Open Source Discrete Element Simulations of Granular Materials Based on Lammps, Supplemental Proceedings, 2011, pp. 781-788.

[31] C. Kloss, C. Goniva, A. Hager, S. Amberger, S. Pirker, Models, algorithms and validation for opensource DEM and CFD–DEM, Progress in Computational Fluid Dynamics, an International Journal, 12 (2012) 140-152.

[32] M. Syamlal, D. Gidaspow, Hydrodynamics of fluidization: Prediction of wall to bed heat transfer coefficients, Aiche Journal, 31 (1985) 127-135.

[33] L. Mu, K.A. Buist, J.A.M. Kuipers, N.G. Deen, Hydrodynamic and Heat Transfer Study of a Fluidized Bed by Discrete Particle Simulations, Processes, 8 (2020) 463.

[34] D.J. Gunn, Transfer of heat or mass to particles in fixed and fluidised beds, International Journal of Heat and Mass Transfer, 21 (1978) 467-476.

[35] Z.Y. Zhou, A.B. Yu, P. Zulli, Particle scale study of heat transfer in packed and bubbling fluidized beds, AIChE Journal, 55 (2009) 868-884.

[36] P. Sauriol, J.V. Pasikhani, J. Shabanian, J. Chaouki, Gas jet penetration in gas-solid fluidized and jetting-fluidized beds - A review, Powder Technology, 421 (2023) 118392.

[37] M.E. Kinaci, T. Lichtenegger, S. Schneiderbauer, A CFD-DEM model for the simulation of direct reduction of iron-ore in fluidized beds, Chemical Engineering Science, 227 (2020) 115858.

[38] Y. Gu, A. Ozel, S. Sundaresan, A modified cohesion model for CFD–DEM simulations of fluidization, Powder Technology, 296 (2016) 17-28.

[39] I. Mema, J. Padding, Fluidization of elongated particles—Effect of multi-particle correlations for drag, lift, and torque in CFD-DEM, AIChE Journal, 67 (2021) e17157.

[40] S. Yang, K. Luo, M. Fang, J. Fan, K. Cen, Influences of operating parameters on the hydrodynamics of a 3-D spout–fluid bed based on DEM modeling approach, Chemical Engineering Journal, 247 (2014) 161–173.

[41] S. Tenneti, R. Garg, S. Subramaniam, Drag law for monodisperse gas–solid systems using particle-resolved direct numerical simulation of flow past fixed assemblies of spheres, International journal of multiphase flow, 37 (2011) 1072-1092.